

## SEDIMENTATION OF PARTICLES IN CONCENTRATED MAGNETIC FLUIDS: NUMERICAL SIMULATION

*A.F. Pshenichnikov, A.A. Kuznetsov*

*Institute of Continuous Media Mechanics, Ural Branch of RAS,  
1 Acad. Korolyov Str., 614013 Perm, Russia*

Gravitational sedimentation of magnetic particles (dipolar hard spheres) is modelled by the means of Monte Carlo method and molecular dynamics. The main result of this simulation is the gradient diffusion coefficient of particles obtained as a function of the particle volume fraction  $\varphi$  ( $\varphi \leq 0.4$ ) at low-to-intermediate coupling constants ( $1 \leq \lambda \leq 4$ ). Based on numerical data it is shown that the applicability range of some previously used analytical models for the diffusion coefficient is mostly limited by  $\lambda \simeq 2$ . A new approximation formula for the diffusion coefficient is proposed. It quite accurately describes the obtained values up to  $\lambda = 4$  and shows an excellent agreement with the known simulation data for the Helmholtz free energy of dipolar spheres.

**Introduction.** Magnetic fluids (MF) are colloidal suspensions of magnetic nanoparticles in a nonmagnetic liquid substrate [1]. The small size of particles (typically of the order of 10–20 nm) provides them with a permanent magnetic moment. Particles are also covered with thin surfactant shells that protect them from coagulation. It is known that mass transfer in MF is rather slow – the initially homogeneous particle distribution may persist for weeks inside a cavity of a few millimeters' height [2]. But eventually, in the absence of convective flux, a stationary inhomogeneous distribution will be established. Three competing processes determine this distribution: gravitational sedimentation, gradient Brownian diffusion and magnetophoresis (the motion of particles in a non-uniform magnetic field). In order to obtain a fluid concentration profile at an arbitrary moment of time, one needs to solve a boundary-value problem including the Maxwell's equations for magnetic field and the dynamic mass transfer equation with a proper consideration of all the above-mentioned processes [3–6]. In the case of a dilute solution, it is possible to neglect interparticle interactions. Then the problem becomes trivial, magnetostatic and diffusion parts can be considered separately and the mass transfer equation can be solved analytically [7, 8]. However, in the case of concentrated fluids, the one-particle approximation is no longer applicable. Steric, magnetodipole and hydrodynamic interparticle interactions affect mass transfer significantly and the magnetic part of the problem becomes tightly interrelated with the diffusive one.

A number of MF mass transfer theories have been proposed during last decades [4, 5, 7–17]. These theories differ by the extent to which sedimentation, diffusion, magnetophoresis, interparticle interactions and transfer anisotropy are taken into account. Here we would appeal to the mass transfer equation derived in [15] in the framework of the simplest dipolar hard sphere (DHS) model, which considers a polar fluid as a gas of impermeable spheres with a point dipolar moment embedded at its center. The corresponding equation describes spatial and temporal variations of the local particle volume fraction  $\varphi$ . Its key advantage is that it does not bound to any specific cavity geometry or applied field orientation.

In the absence of convective flows it might be written as follows:

$$\frac{\partial \varphi}{\partial t} = -\operatorname{div} \left\{ D_0 K(\varphi) \left( \varphi L(\xi_e) \nabla \xi_e + \varphi G_\gamma \hat{\mathbf{g}} - \frac{D(\lambda, \varphi)}{D_0 K(\varphi)} \nabla \varphi \right) \right\}. \quad (1)$$

Here,  $D_0 = b_0 kT$  is the Einstein's diffusion coefficient for a Brownian particle in a dilute solution,  $K(\varphi) = b(\varphi)/b_0$  is the relative particle mobility,  $b(\varphi)$  and  $b_0$  are the particle mobility in a magnetic and in a carrier fluid, respectively. Strictly, the functions  $b(\varphi)$  and  $K(\varphi)$  should be tensors as the particle mobility in the magnetic field is anisotropic. But it was demonstrated in [14] that the influence of the mobility anisotropy in MF is an order of magnitude weaker than the influence of the thermodynamic forces' anisotropy, which is accounted for by the first term in Eq. (1). This term is responsible for magnetophoresis,  $L(x) = \coth(x) - 1/x$  is the Langevin function,  $\xi_e = \mu_0 \mu H_e / kT$  is the Langevin parameter,  $\mu_0 = 4 \times 10^{-7}$  H/m,  $\mu$  is the particle magnetic moment,  $kT$  is the thermal motion energy.  $H_e$  is the effective magnetic field acting on a probe particle. It is determined not only by the macroscopic magnetic field  $H$  inside the cavity, but also by the local particle concentration. The accuracy of this effective field approximation depends mainly on the choice of  $H_e = H_e(H, \varphi)$  function. Authors of [15] themselves have used the second-order modified mean-field theory. A detailed model description is offered in [18, 19]. The second term in Eq. (1) is related to gravitational sedimentation,  $G_\gamma$  is the gravitational parameter, which equals to the inverse barometric distribution height,  $\hat{\mathbf{g}}$  is a unit vector in the direction of the gravitational field. Finally, the coefficient in front of  $\nabla \varphi$  is the effective isotropic diffusion coefficient of magnetic particles:

$$\frac{D(\lambda, \varphi)}{D_0 K(\varphi)} = 1 + \frac{2\varphi(4 - \varphi)}{(1 - \varphi)^4} + \frac{\Delta D(\lambda, \varphi)}{D_0 K(\varphi)}. \quad (2)$$

The second term in this expression accounts for steric interactions and is derived in the Carnahan–Starling approximation for the hard sphere (HS) equation of state [20]. The third term is responsible for magnetodipole interactions,  $\lambda = \mu_0 \mu^2 / 4\pi \sigma^3 kT$  is the dipolar coupling constant,  $\sigma$  is the particle diameter. Henceforth, we will use dimensionless quantities  $\hat{D} = D(\lambda, \varphi) / D_0 K(\varphi)$  and  $\Delta \hat{D} = \Delta D(\lambda, \varphi) / D_0 K(\varphi)$ .

Several analytical models for  $\Delta \hat{D}$  are currently available in the literature. A brief review of the main expressions is given in the next section. Some of these expressions have already been involved in the solution of complex applied problems. At the same time, their accuracy has been estimated only roughly and implicitly. Multiple features of the real magnetic fluids, which differ it from the idealized DHS model (polydispersity, van der Waals interactions and partial aggregation due to defects of the particle protective shells), complicate thorough comparison between theory and experiment. On the other hand, even the simple DHS model has its own features that need to be properly considered in numerical investigation. For example, it is known that at  $\lambda \geq 3$  dipolar spheres have a tendency to assemble into short chains [29], and one can expect that these objects impact significantly on the mass transfer processes in the system. So, in this work, we will use molecular dynamics and Monte Carlo simulation techniques. The key advantage of these methods is that they automatically allow us to take into account all various effects of dipole-dipole interactions, including association phenomena. We will calculate the diffusion coefficient of DHS systems with low to intermediate coupling constants  $1 \leq \lambda \leq 4$ . Based on the obtained data we will determine applicability limits of the existing DHS diffusion models and will attempt to come up with a new reliable approximation formula for  $\Delta \hat{D}$ .

**1. Analytical expressions for  $\Delta\hat{D}(\lambda, \varphi)$ .** In [11, 12], the DHS diffusion coefficient has been first presented in the form of Eq. (2). Authors also derived the magnetodipole correction in the linear approximation with respect to  $\varphi$ :

$$\Delta\hat{D}(\lambda, \varphi) = -\frac{8}{3}\lambda^2\varphi. \quad (3)$$

Eq. (3) illustrates the fact that the magnetodipole interactions play a role of effective attraction between particles and cause a decrease of the diffusion coefficient. A more profound expression is proposed in [21]:

$$\Delta\hat{D}(\lambda, \varphi) = -\frac{8}{3}\frac{\lambda^2\varphi}{(1 + 1.25\lambda\varphi)^2}. \quad (4)$$

Eq. (4) was used by authors as a basis for a more complex mass transfer theory that takes into account partial aggregation of MF. This theory demonstrates good agreement with experimental results, but is supposed to be valid only for relatively small values of the coupling constant  $\lambda \leq 1$ . Eq. (4) was derived purely heuristically, whereas a more common way is a thermodynamic approach. Eq. (2) was derived from the general Batchelor's equation for the gradient diffusion coefficient of interacting colloidal particles in solution [22]:

$$D = b(\varphi)\frac{\varphi}{1 - \varphi} \left( \frac{\partial\mu_c}{\partial\varphi} \right)_{p,T}, \quad (5)$$

where  $\mu_c$  is the chemical potential of particles. It can be shown using Eq. (5) and the expression for the Gibbs free energy of magnetic fluid [11, 12] that the following relation is valid:

$$\Delta\hat{D}(\lambda, \varphi) = \varphi \frac{\partial^2}{\partial\varphi^2} \left( \varphi \frac{\Delta F(\lambda, \varphi)}{NkT} \right), \quad (6)$$

where  $N$  is the particle number and  $\Delta F(\lambda, \varphi) = F(\lambda, \varphi) - F^{HS}(\varphi)$  is the magnetodipole correction to the Helmholtz free energy of particles. An exact expression for the DHS free energy is absent for the moment. In [15], the following approximation has been constructed:

$$\frac{\Delta F(\lambda, \varphi)}{NkT} = -\frac{4}{3}\lambda^2\varphi \frac{(1 + 0.04\lambda^2)}{(1 + 0.308\lambda^2\varphi)} \frac{(1 + 1.28972\varphi + 0.72543\varphi^2)}{(1 + 0.83333\lambda\varphi)}. \quad (7)$$

The comparison of Eq. (7) with known numerical results for the free energy has demonstrated a good agreement at least up to  $\lambda = 2$  and  $\varphi = 0.4$ . In [23, 24], Eq. (7) in combination with Eqs. (1) and (6) was actively involved in numerical studies of magnetic particles' sedimentation under the action of gravitational and magnetic fields. The results reported here can help to specify applicability limits of [23, 24] conclusions.

Among different theoretical approaches to the DHS free energy, we will focus on the "logarithmic free energy" (LFE) theory recently developed in [25, 26]. In this theory, the DHS free energy is represented with respect to that of the HS system by a logarithmic equation and the argument of the logarithm is a polynomial expansion in  $\varphi$  with coefficients depending on  $\lambda$ . The first three coefficients are restored from the known terms of the DHS equation of state virial expansion and the resulting expression is

$$\frac{\Delta F(\lambda, \varphi)}{NkT} = -\ln \left( 1 + \sum_{n=1}^3 n^{-1} I_n(\lambda) \varphi^n \right), \quad (8)$$

$$I_1 = \frac{4}{3}\lambda^2 + \frac{4}{75}\lambda^4 + \frac{116}{55125}\lambda^6, \quad (9)$$

$$I_2 = \left(4 \ln 2 + \frac{2}{3}\right) \lambda^2 - \frac{20}{9} \lambda^3 + \left(\frac{661727}{9600} - \frac{1468}{15} \ln 2\right) \lambda^4 - 0.155 \lambda^5 + 0.111 \lambda^6 - 0.0143 \lambda^7 + 0.0105 \lambda^8 - 0.00146 \lambda^9 + 0.000677 \lambda^{10} - 0.00013 \lambda^{11} + 0.0000464 \lambda^{12}, \quad (10)$$

$$I_3 = 2.901720 \lambda^2. \quad (11)$$

Eq. (8) shows a close agreement with the numerically obtained  $\Delta F$  values in a wide concentration range at  $\lambda \leq 2$  and a correct low-density ( $\varphi \leq 0.1$ ) behavior at  $\lambda = 3$  and  $\lambda = 4$ . In general, the LFE theory demonstrates an advantage over other existing approaches, such as the direct virial expansion or the thermodynamic perturbation theory. However, LFE predictions for the chemical potential seem to be slightly less accurate than for the free energy. Its precision for the diffusion coefficient is to be determined.

**2. Simulation details.** The simulated system is a finite size cylinder of volume  $V = \pi R^2 L$  with rigid walls filled with  $N$  magnetic particles (see Fig. 1). The system is placed in the gravitational field (with a unit vector  $\hat{\mathbf{g}}$ ), the magnetic field is absent and the relative permeability of the cylinder environment is unity (vacuum boundary conditions). Each particle is characterized by its center position  $\mathbf{r}_i = \sigma \hat{\mathbf{r}}_i$  and by the dipole moment orientation  $\boldsymbol{\mu}_i = \mu \hat{\boldsymbol{\mu}}_i$ . The energy of the  $i^{\text{th}}$  particle is given by the expression

$$\frac{U_i}{kT} = G_\gamma z_i + \sum_{\substack{j=1 \\ i \neq j}}^N \left( \frac{u^{SR}(r_{ij})}{kT} - \lambda \left[ \frac{3(\hat{\boldsymbol{\mu}}_i \hat{\mathbf{r}}_{ij})(\hat{\boldsymbol{\mu}}_j \hat{\mathbf{r}}_{ij})}{\hat{r}_{ij}^5} - \frac{\hat{\boldsymbol{\mu}}_i \hat{\boldsymbol{\mu}}_j}{\hat{r}_{ij}^3} \right] \right) + \sum_{\text{walls}} \frac{u_i^w}{kT}. \quad (12)$$

Here, the first term is the gravitational potential,  $\hat{\mathbf{r}}_{ij} = \hat{\mathbf{r}}_i - \hat{\mathbf{r}}_j$ ,  $u^{SR}$  is the short-range steric repulsion potential, its precise form for the case of the DHS system is the hard sphere potential

$$u^{HS}(r) = \begin{cases} \infty & \text{if } r < \sigma \\ 0 & \text{if } r \geq \sigma \end{cases}, \quad (13)$$

the expression in square brackets is the dipole-dipole interaction energy, the last term denotes interactions with cylinder boundaries, for each cylinder wall  $u_i^w = u^{SR}(2r_i^w)$ , where  $r_i^w$  is the distance between the particle center and the closest point of the wall. Input parameters of the simulation are the particle number  $N$ , the coupling constant  $\lambda$ , the mean volume fraction  $\langle \varphi \rangle = (\pi \sigma^3 / 6) N / V$ , the

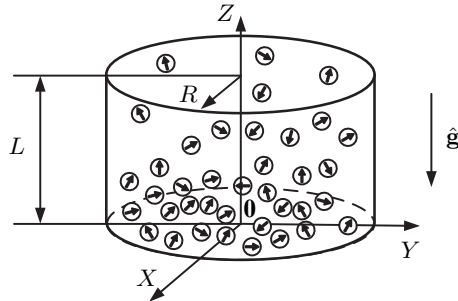


Fig. 1. Schematic presentation of the simulated system.

gravitational parameter  $G_\gamma$ , and the cylinder length  $L$  (always divisible by  $\sigma$ ). The output of the simulation is an equilibrium concentration profile along the cylinder axis ( $\varphi = \varphi(z)$ ).

Two methods were used to achieve the equilibrium state of the system. The first one was the Monte Carlo method in the standard form of Metropolis algorithm for NVT ensemble [27, 28]. One simulation step consisted of  $N$  attempts to change the state of a randomly picked particle (the state change included random rotation and random transition). The other method was the Langevin molecular dynamics [19, 27]. Particle equations of motion were identical to those in [19]. Most of the simulations were performed with  $G_\gamma L = 5$ . The coupling constant  $\lambda$  was varied between 0 and 4, the mean volume fraction  $\langle \varphi \rangle$  between 0.01 and 0.36. The maximum number of particles in the MC experiments was  $N = 1024$  and in MD it was  $N = 32768$ . The  $\varphi(z)$  values in MC simulations were typically averaged over  $10^6$  simulation steps after  $5 \times 10^5$  steps for equilibration. The MD simulation usually consisted of  $1.6 \times 10^6$  time steps for  $N \leq 16384$  and of  $0.5 \times 10^6$  time steps for  $N = 32768$ ; the maximum equilibration period was  $5 \times 10^5$  steps. The motivation to use the two methods is as follows. Hard sphere repulsion (Eq. (13)) can be easily realized in the Metropolis algorithm, but for MD it was more efficient to use a continuous computable approximation. We used the following expression based on the Weeks–Chandler–Andersen soft sphere potential [30]:

$$u^{SR}(r)/kT = \begin{cases} 4 [(\sigma/r)^{48} - (\sigma/r)^{24}] + 1 & \text{if } r < 2^{1/24}\sigma \\ 0 & \text{if } r \geq 2^{1/24}\sigma \end{cases}, \quad (14)$$

Tentative MC and MD simulations with  $N = 1024$  were performed to ensure that the approximation (14) is enough to reproduce the results obtained with a true HS potential. So MC simulations were used only as a reference point for molecular dynamics. All the numerical results given in the next section are from MD.

Concentration profiles were obtained as sets of points ( $z_i = (0.5 + i)\sigma, \varphi_i^*$ ),  $i = 0 \dots L/\sigma - 1$ , where  $\varphi_i^*$  is the particle volume fraction inside a thin layer between the planes  $z = z_i \pm 0.5\sigma$ . It was also necessary to remember that near the boundaries the local volume fraction gradually drops to zero due to the wall and particle impermeability. To take it into account, we excluded the upper and the lower layers from consideration and for the remaining layers we renormalized the calculated concentrations  $\varphi_i^*$  by the rule:

$$\varphi_i = \varphi_i^* R^2 / (R - \delta)^2, \quad (15)$$

where  $R$  is the cylinder radius and  $\delta = 0.15\sigma$  is a fitting parameter. Its value was chosen to minimize the discrepancy between the simulation results for  $\lambda = 0$  and the Carnahan–Starling approximation.

**3. Results and discussion.** No magnetic field was applied in our system. We also ensured that a net spontaneous magnetization did not take place: the reduced order parameters  $M \langle \left| \sum_i^N \hat{\mu}_i \right| \rangle / N$  and  $M_{tor} = \langle \left| \sum_i^N [r_i \times \hat{\mu}_i] / r_i \right| \rangle / N$  were much smaller than unity in the entire investigated range of concentrations ( $\varphi \leq 0.4$ ), particle numbers ( $N \leq 32784$ ) and coupling constants ( $\lambda \leq 4$ ). So we can neglect the magnetophoresis term in Eq. (1), and the implicit equation for the static concentration profile  $\varphi = \varphi(z)$  can be written as follows,

$$\hat{D}(\lambda, \varphi) = -\frac{\varphi G_\gamma}{\partial \varphi / \partial z} = -\frac{G_\gamma}{\partial \ln \varphi / \partial z}. \quad (16)$$

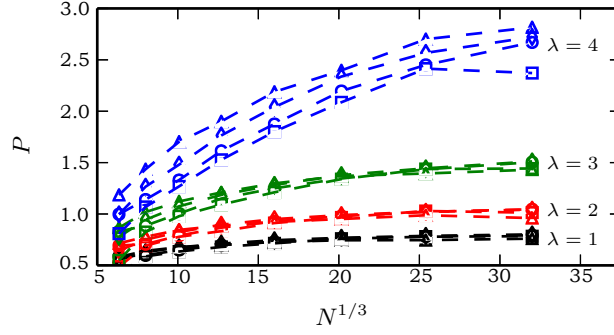


Fig. 2. The segregation coefficient  $P$  as a function of the particle number for cylinders with heights  $L = 20\sigma$  (triangles),  $L = 40\sigma$  (diamonds),  $L = 60\sigma$  (circles) and  $L = 80\sigma$  (squares) at different  $\lambda$ .  $\langle\varphi\rangle = 0.25$ .

The equilibrium state of the considered system is inhomogeneous, and for this reason we did not use conventional periodic boundary conditions schemes [27, 28]. It gave rise to the well-known thermodynamic limit problem: due to the long-range nature of dipole-dipole interactions, relatively small systems containing hundreds or thousands of particles are not identical in properties to thermodynamically large systems, which are really of interest. To understand how the system sizes affect the equilibrium spatial distribution, we collected a large set of profiles for different values of  $N$  and  $L$ . For all of the profiles  $\langle\varphi\rangle = 0.25$  and  $G_\gamma L = 5$ ,  $N$  was varied from 256 to 32768,  $L$  was varied from  $20\sigma$  to  $80\sigma$ . For every profile we calculated the segregation coefficient

$$P = \frac{\varphi(L/8) - \varphi(7L/8)}{\varphi(7L/8)}. \quad (17)$$

Obviously, in the thermodynamic limit,  $\hat{D}$  does not depend on the system sizes. It is easy to see from Eq. (16) that in this case the cylinder elongation from some  $L_0$  to  $L = \alpha L_0$  will only “stretch” the profile along the  $z$ -axis ( $\varphi(z) = \varphi_0(z/\alpha)$ ) if  $\langle\varphi\rangle$  and  $G_\gamma L$  remain constant. Then  $P$  should not depend on the sizes either. Fig. 2 depicts dependences of  $P$  on  $N$  at different  $L$  and  $\lambda$ . The plots illustrate a strong impact of the dipole-dipole interactions on the sedimentation processes in the system. With  $\lambda$  changing from 1 to 4, the segregation coefficient increases almost four times. The influence of the cylinder elongation on the concentration distribution seems to be considerably small. Differences at  $\lambda = 4$  are caused by the fact that at such high coupling constants the allocated equilibration time is not sufficient for long cylinders with  $L > 40\sigma$ . It can be seen that the curves approach an asymptote at  $N > 25^3$ . In all subsequent calculations,  $N$  was set to 16384 and  $L$  was set to  $20\sigma$ ,  $G_\gamma L = 5$ .

The calculated concentration profiles for  $\langle\varphi\rangle = 0.15$  and  $\lambda = 1 \dots 4$  are shown in Fig. 3. The theoretical curves for the given  $\lambda$  and  $\langle\varphi\rangle$  are drawn by the means of Eq. (16). For  $\lambda = 1$  and  $\lambda = 2$ , the agreement between the theory and the simulation is rather good. At  $\lambda = 3$ , the discrepancy starts to rise, and for  $\lambda = 4$  the numerically obtained and analytically predicted profiles differ qualitatively from each other. The reason is that every model under consideration predicts that at some point the diffusion coefficient of the system becomes zero. It might be considered as a condition of spinodal decomposition, when the system stratifies into weakly and strongly concentrated phases. The corresponding critical point  $(\lambda^*, \varphi^*)$  for the heuristic model (4) is (4.15, 0.064), for the approximation (7), this

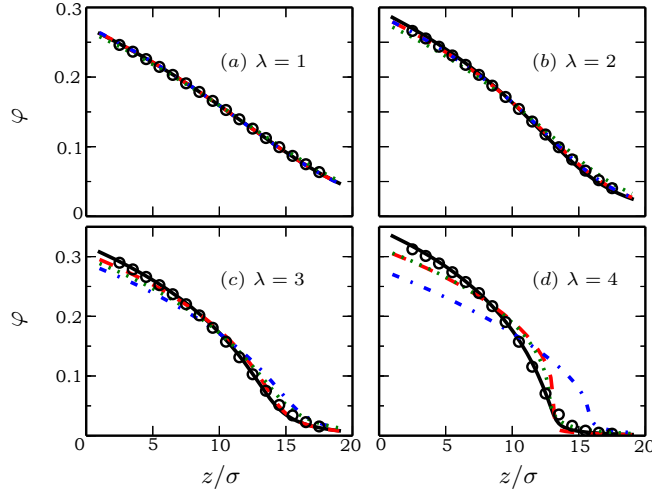


Fig. 3. Static concentration profiles for systems with different  $\lambda$ .  $\langle\varphi\rangle = 0.15$ . Points are simulation data, solid lines are from the new approximation (2), (18); dotted lines are from the heuristic model (2), (4); dot-dashed lines are from the approximation (2), (6), (7); dashed lines are from the LFE theory (2), (6), (8).

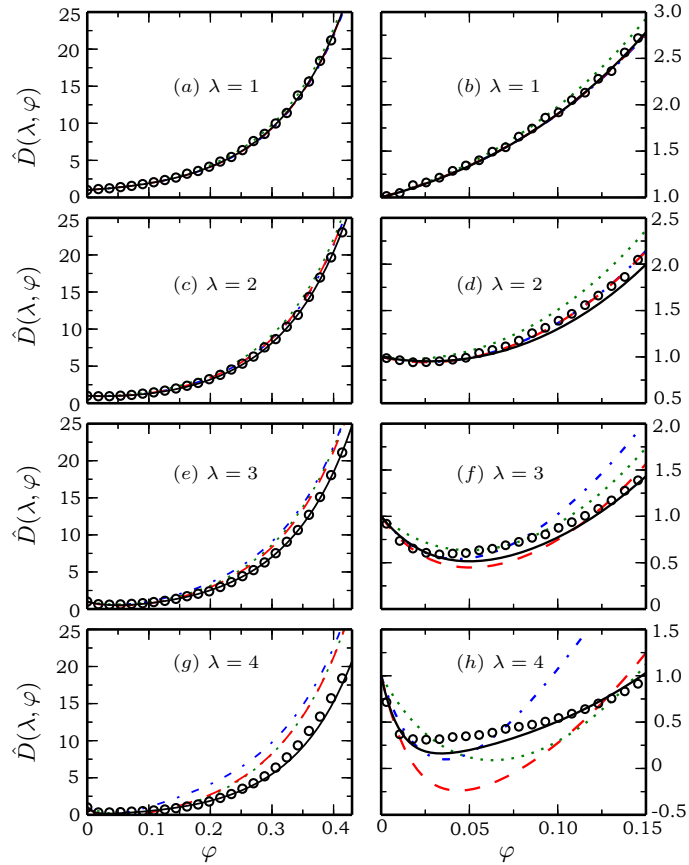
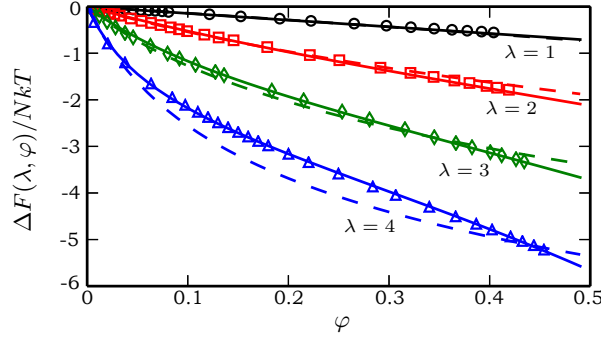


Fig. 4. The gradient diffusion coefficient  $\hat{D}$  as a function of the local volume fraction  $\varphi$  for systems with different  $\lambda$ . Data are shown in two scales,  $\varphi \leq 0.43$  and  $\varphi \leq 0.15$ . Points are simulation data, solid lines are from the new approximation (2), (18); dotted lines are from the heuristic model (2), (4); dot-dashed lines are from the approximation (2), (6), (7); dashed lines are from the LFE theory (2), (6), (8).



*Fig. 5.* Difference between the Helmholtz free energy of DHS and HS systems  $\Delta F/NkT$  as a function of the volume fraction  $\varphi$  for different coupling constants  $\lambda$ . Points are the MC results from [25]; dashed lines are from the LFE theory (8); solid lines are from the new approximation ((6) and (18)).

is (4.22, 0.034), and for the LFE theory (8) it is (3.64, 0.049). At  $\lambda = 4$  (Fig. 3d), the system is already stratified according to the LFE theory and in the precritical state according to other two models. At the same time, our simulated system does not demonstrate evidences of phase separation.

In order to obtain the diffusion coefficient, we calculated a large number of profiles with different  $\langle \varphi \rangle$ , interpolated them with splines and estimated values of  $\partial \ln \varphi / \partial z$  by using the central difference formula. Then  $\hat{D}(\lambda, \varphi)$  values were derived from Eq. (16). Fig. 4 depicts dependences of  $\hat{D}(\lambda, \varphi)$  on  $\varphi$  at different  $\lambda$ . For  $\lambda = 1$ , all the models fit the data generally well. For  $\lambda = 2$ , the heuristic model (4) gives a small but noticeable overestimation at  $\varphi > 0.1$ . At  $\lambda = 3$ , the mismatch between the simulation and the theories is more distinct, it starts from  $\varphi = 0.1$ – $0.15$  and achieves  $\sim 15\%$  at  $\varphi = 0.4$ . At  $\lambda = 4$ , the theory seriously overestimates the diffusion coefficient at  $\varphi > 0.1$  and underestimates it at  $0.01 < \varphi < 0.1$ , which is especially true for the LFE theory as it predicts negative values of  $\hat{D}$  within this range. The simplest model (4) at  $\lambda = 4$  incorrectly describes even the linear portion of the numerical curve, whereas the applicability of the models (7) and (8) is limited only by extremely small volume fractions of the order of one percent. Trying to fit the presented data with some analytical expression, we constructed the following approximation:

$$\Delta \hat{D}(\lambda, \varphi) = - [1 - \exp(- [3\lambda^2 - 0.1\lambda^4 + 0.018\lambda^6] \varphi)] \exp(1.3\lambda\varphi). \quad (18)$$

Despite that Eq. (18) predicts a wrong linear behaviour at  $\varphi \rightarrow 0$ , in practice it provides a good precision in the whole range of the studied concentrations up to  $\lambda = 3$ . At  $\lambda = 4$ , Eq. (18) closely traces numerical results and is still suitable for estimates. To verify the formula, we calculated the corresponding free energy correction  $\Delta F/NkT$  with the help of Eq. (6). Fig. 5 shows that the agreement between the new approximation and the MC results for  $\Delta F/NkT$  from [25] is excellent.

**4. Conclusion.** In this work, we have numerically investigated the process of gravitational sedimentation in a concentrated system of dipolar hard spheres. We have obtained a series of equilibrium concentration profiles for systems with different mean volume fractions  $\langle \varphi \rangle$  and coupling constants  $\lambda$ . Using these data and the mass transfer Eq. (1), we calculated values of the DHS gradient isotropic diffusion coefficient (Eq. (2)). Three analytical models were compared with our data: the heuristic model derived in [21] (Eqs. (2) and (4)), the approximation from [15]

(Eqs. (2), (6) and (7)) and the “logarithmic free energy” theory (Eqs. (2), (6) and (8)). The comparison has demonstrated that all the models work generally well for the coupling constants  $\lambda = 1$  and  $\lambda = 2$ , though the latter two models are expectedly more accurate. At  $\lambda > 3$ , all the models give a significant overestimation at high concentrations  $\varphi > 0.1$  and underestimate numerical data at  $\varphi \sim 0.01 - 0.1$ . In this range of low concentrations, the analytical models predict a system spinodal decomposition ( $\hat{D} \leq 0$ ) at  $\lambda \simeq 4$ , whereas no evidences of phase separation have been found in the simulations. In particular, this means that the predictions of [23, 24] for  $\lambda > 3$  should probably be treated with caution. A new approximation for the DHS diffusion coefficient has been proposed (Eqs. (2) and (18)). It is in good agreement with our and other authors’ numerical results at  $\lambda \leq 4$  and  $\varphi \leq 0.4$ . In our opinion, it would be a suitable choice for the forthcoming studies of concentrated magnetic fluids. A detailed study of the mass transfer processes in magnetic fluids with higher coupling constants ( $\lambda > 4$ ) will be the subject of a future publication.

**Acknowledgements.** This research was supported by the Ural Branch of the RAS (project No. 12-T-1-1008) and by the Russian Foundation for Basic Research (grants No. 13-02-00076 and No. 14-01-96007). Calculations were performed using the “Uran” supercomputer of IMM UB RAS.

## REFERENCES

- [1] R.E. ROSENSWEIG. *Ferrohydrodynamics*. (Cambridge University Press, New York, 1985).
- [2] M.I. SHLIOMIS. Magnetic fluids. *Sov. Phys. Usp.*, vol. 17 (1974), no. 2, pp. 153–169 (in Russian).
- [3] E.YA. BLUMS, M.M. MAYOROV, AND A.O. CEBERS. *Magnetic Fluids* (Walter de Gruyter, Berlin, 1997).
- [4] V. FRISHFELDS AND E. BLUMS. Microconvection and mass transfer near bodies in non-uniformly magnetized ferrofluid. *Magnetohydrodynamics*, vol. 41 (2005), no. 4, pp. 361–366.
- [5] V.G. BASHTOVOI *et al.* Influence of Brownian diffusion on statics of magnetic fluid. *Magnetohydrodynamics*, vol. 43 (2007), no. 1, pp. 17–26.
- [6] V.G. BASHTOVOI *et al.* The effect of magnetophoresis and Brownian diffusion on the levitation of bodies in a magnetic fluid. *Magnetohydrodynamics*, vol. 44 (2008), no. 2, pp. 121–126.
- [7] A.S. IVANOV AND A.F. PSHENICHNIKOV. Magnetophoresis and diffusion of colloidal particles in a thin layer of magnetic fluids. *J. Magn. Magn. Mat.*, vol. 322 (2010), pp. 2575–2580.
- [8] A.S. IVANOV, A.F. PSHENICHNIKOV. Dynamics of magnetophoresis in dilute magnetic fluids. *Magnetohydrodynamics*, vol. 46 (2010), no. 2, pp. 125–136.
- [9] A.O. TSEBERS. Nonlinear magnetodiffusion problems in the intrinsic field of a particle ensemble. *Magnetohydrodynamics*, vol. 27 (1991), no. 2, pp. 123–128.
- [10] I. DRIKIS, A. CEBERS. Pattern formation at magnetophoretic motion in the self-magnetic field of magnetic colloid. *Magnetohydrodynamics*, vol. 47 (2011), no. 1, pp. 3–10.
- [11] YU.A. BUEVICH, A.YU. ZUBAREV, AND A.O. IVANOV. Brownian diffusion in concentrated ferrocolloids. *Magnetohydrodynamics*, vol. 25 (1989), no. 2, pp. 172–176.
- [12] A.O. IVANOV. Phase stratification of magnetic fluids. PhD Thesis, Ural State University, Ekaterinburg, 1998. (in Russian).

- [13] K.I. MOROZOV. The translational and rotational diffusion of colloidal ferroparticles. *J. Magn. Magn. Mat.*, vol. 122 (1993), pp. 98–101.
- [14] K.I. MOROZOV. Gradient diffusion in concentrated ferrocolloids under the influence of a magnetic field. *Phys. Rev. E*, vol. 53 (1996), pp. 3841–3846.
- [15] A.F. PSHENICHNIKOV, E.V. ELFIMOVA, AND A.O. IVANOV. Magnetophoresis, sedimentation, and diffusion of particles in concentrated magnetic fluids. *J. Chem. Phys.*, vol. 134 (2011), pp. 184508–1–9.
- [16] J.-C. BACRI *et al.* Forced Rayleigh experiment in a magnetic fluid. *Phys. Rev. Lett.*, vol. 74 (1995), pp. 5032–5035.
- [17] J.-C. BACRI *et al.* Transient grating in a ferrofluid under magnetic field: effect of magnetic interactions on the diffusion coefficient of translation. *Phys. Rev. E*, vol. 52 (1995), pp. 3936–3942.
- [18] A.O. IVANOV AND O.B. KUZNETSOVA. Magnetogranulometric analysis of ferrocolloids: second-order modified mean field theory. *Colloid J.*, vol. 68 (2006), no. 4, pp. 472–483.
- [19] A.O. IVANOV *et al.* Magnetic properties of polydisperse ferrocolloids: a critical comparison between experiment, theory, and computer simulation. *Phys. Rev. E*, vol. 75 (2007), pp. 061405–01–12.
- [20] N.F. CARNAHAN AND K.E. STARLING. Equation of state for nonattracting rigid spheres. *J. Chem. Phys.*, vol. 51 (1969), pp. 635–636.
- [21] A.F. PSHENICHNIKOV AND A.S. IVANOV. Magnetophoresis of particles and aggregates in concentrated magnetic fluids. *Phys. Rev. E*, vol. 86 (2012), pp. 051401–1–11.
- [22] G.K. BATCHELOR. Brownian diffusion of particles with hydrodynamic interaction. *J. Fluid Mech.*, vol. 74 (1976), no. 1, pp. 1–29.
- [23] A.F. PSHENICHNIKOV AND E.N. BURKOVA. Effect of demagnetizing fields on particle spatial distribution in magnetic fluids. *Magnetohydrodynamics*, vol. 48 (2012), no. 3, pp. 503–514.
- [24] A.F. PSHENICHNIKOV AND E.N. BURKOVA. Forces acting on a permanent magnet placed in a rectangular cavity with a magnetic fluid. *Computational Continuum Mechanics*, vol. 7 (2014), no. 1, pp. 5–14.
- [25] E.A. ELFIMOVA, A.O. IVANOV, AND P.J. CAMP. Thermodynamics of dipolar hard spheres with low-to-intermediate coupling constants. *Phys. Rev. E*, vol. 86 (2012), pp. 021126–1–9.
- [26] E.A. ELFIMOVA, A.O. IVANOV, P.J. CAMP. Thermodynamics of ferrofluids in applied magnetic fields. *Phys. Rev. E*, vol. 88 (2013), pp. 042310–01–11.
- [27] M.P. ALLEN AND D.J. TILDESLEY. *Computer Simulation of Liquids*. (Clarendon Press, Oxford, 1987).
- [28] D. FRENKEL AND B. SMIT. *Understanding Molecular Simulation: from Algorithms to Applications*. (Academic Press, San Diego, 2002).
- [29] Z. WANG, C. HOLM, AND H.W. MÜLLER. Molecular dynamics study on the equilibrium magnetization properties and structure of ferrofluids. *Phys. Rev. E*, vol. 66 (2002), pp. 021405–01–13.
- [30] J.D. WEEKS, D. CHANDLER, AND H.C. ANDERSEN. Role of repulsive forces in determining the equilibrium structure of simple liquids. *J. Chem. Phys.*, vol. 54 (1971), pp. 5237–5247.

Received 21.01.2015